Unraveling the Mechanism of Near-Infrared Thermally Activated Delayed Fluorescence of TPA-Based Molecules: Effect of Hydrogen Bond Steric Hindrance

Can Leng, Sheng You, Yubing Si,* Hai-Mei Qin, Jie Liu, Wei-Qing Huang, and Keqin Li*

ACCESS | Metrics & More | Article Recommendations | Supporting Information

ABSTRACT: A recently synthesized novel molecule (named CAT-1) exhibits intriguing near-infrared (NIR) thermally activated delayed fluorescence (TADF) close to 1000 nm wavelength; however, the mechanism behind these intrinsic properties is not fully understood. Herein, we unravel that the fluorescence emission spectrum with a broad wavelength range (770−950 nm) of CAT-1 is primarily induced by hydrogen bond steric hindrance based on density functional theory and Marcus theory. It is found that the hydrogen bond steric hindrance plays a critical role in inhibiting the twist of the configuration of different excited states, which leads to the minor driving force for fast electron trapping between the excited states, as well as small internal reorganization energy caused by less changed geometric configuration. Furthermore, such steric hindrance will cause a more distorted plane, resulting in a less favorable electron delocalization. A faster reverse intersystem crossing (RISC) rate is then obtained due to the nearly unchanged conformation between excited states caused by steric hindrance, although the spin−orbit coupling is small. Consequently, the NIR TADF with a longer wavelength can be emitted in CAT-1. This work shows that the hydrogen bond steric hindrance can fine-tune the electronic interactions of the donor and acceptor units to control the TADF.
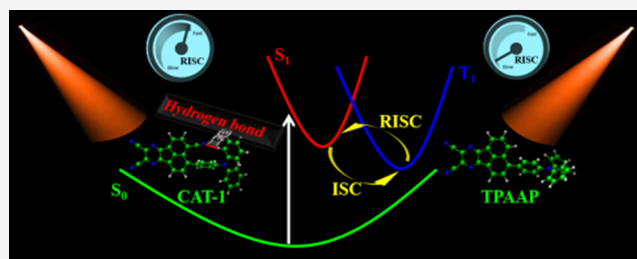
1. INTRODUCTION

Organic light-emitting devices (OLEDs) that produce visible and near-infrared (NIR) electroluminescence (EL) have offered extensive applications in photovoltaics and photocatalysis fields.[1−5] As one of the most promising OLED materials, thermally activated delayed fluorescence (TADF) emitters are now being considered as the third generation of OLED materials.[6] OLEDs are capable of producing EL with highly desirable features of color tunability, fabrication flexibility, and low cost by radiative decay from the organic compound film layer to respond to the electrical current.[4−9] For TADF OLEDs, the breakthrough by Adachi's group toward high-performance and low-cost OLEDs paves the way for the successor with a theoretical maximum internal quantum efficiency (IQE) of 100% due to overcoming the theoretical limit (25%) of spin statistics in the absence of heavy transition metals.[5]

Generally, efficient OLEDs can emit three primary colors: red, green, and blue.[10,11] In the past decades, major interests have focused on green and blue organic emitters with an external quantum efficiency (EQE) of over 30%.[5,12,13] Recent studies are being directed to red and even NIR TADF emitters because of their burgeoning digital displays in devices such as sensors, night vision, telecommunications, photodetectors, and NIR bioimaging.[14−19] In the design of efficient TADF emitters, rigorous molecular considerations are indispensable. The basic requirements rely on a small energy gap (ΔE_{ST}) between the first singlet state (S_1) and the triplet state (T_1) for effective upconversion from T_1 to S_1, which can be realized by the reduction in the overlap of the highest occupied molecular orbital (HOMO) and the lowest unoccupied molecular orbital (LUMO), as well as the large energy gap between S_1 and the ground state S_0 for high luminescent utility.[20,21] Furthermore, for NIR TADF emitters, an twist between the donor (D) and acceptor (A) units is indispensable since the long-wavelength emitters generally suffer the increasing nonradiative decay governed by inhibiting the external quantum efficiency (EQE) and energy gap law.[22,23] Therefore, high rigidity in long-wavelength TADF emitters is desired for constructing efficient NIR TADF emitters.

The molecules with triphenylamine (TPA)-based donors (D) are one of the most promising NIR TADF candidates. For example, Adachi et al. have reported two TPA-based TADF emitters with the maximum EQE of newly 10%, ranging the wavelengths of 780 nm and above 800 nm, respectively.[24,25] A

D-A
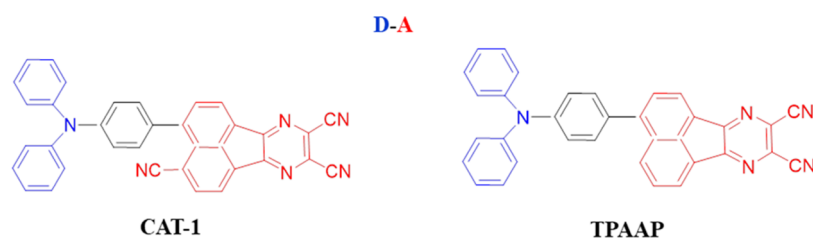
Figure 1. Structure schema of TADF molecules with (left) and without (right) the CN group.

Table 1. Comparison of Different Hybrid Functional Methods for Electrooptic Properties of CAT-1 and TPAAP[a]

molecules	functional	HOMO/LUMO/E_g (eV)	λ_{abs} (nm)	λ_{em} (nm)	$E_S/E_T/\Delta E_{ST}$ (eV)
CAT-1	B3LYP	−5.45/−3.76/1.68 (−5.64/−4.11/1.53)	584(578)	837(887)	1.194/1.192/0.002 (1.24/1.20/0.04)
	PBE0	−5.73/−3.67/2.06	510	717	1.344/1.341/0.003
	M062X	−6.57/−3.03/3.54	506	627	2.318/1.841/0.477
TPAAP	B3LYP	−5.40/−3.11/2.29 (−5.38/−3.39/1.99)	487(487)	681(705)	1.812/1.611/0.202 (2.28/2.09/0.19)
	PBE0	−5.63/−3.08/2.55	588	620	1.999/1.634/0.366
	M062X	−6.54/−2.41/4.13	426	466	2.657/1.975/0.682

[a]Multiple electronic parameters are calculated by the TDDFT method at three different hybrid functionals. These parameters include the energy of HOMO, LUMO, E_g ($E_g = E_{HOMO} - E_{LUMO}$), the absorption λ_{abs} and emission λ_{em} wavelength, and the energy of singlet and triplet excited state with its energy gap $E_S/E_T/\Delta E_{ST}$. The experimental values are listed in the bracket.

over 10% EQE TPA-based TADF has been developed by Yuan et al. with a peak wavelength of 756 nm.[26,27] Recently, a novel NIR TADF 3-triphenylamine-4-cyano-acenaphtho[1,2-b]-pyrazine-8,9-dicarbonitril (CAT-1) in a single acceptor (A) with a TPA-based donor has been reported to have a wavelength of nearly 1000 nm.[28] It is generally assumed that the functioning of OLED is dominantly determined by an effective intersystem crossing (ISC) process with "singlet-trapping" to the emitted T_1 state, as well as a reverse ISC (RISC) process with "triplet-trapping" to the S_1 state.[10,11] However, the mechanism of the NIR TADF of this CAT-1 molecule is not fully understood.

Here, we have theoretically studied the electronic structure and the electrooptic properties of two TPA-based NIR TADF emitters by the density functional theory (DFT)[29] and time-dependent DFT (TDDFT)[30] methods. Marcus formula is chosen to explore the electron transfer and trapping (the ISC and RISC) processes based on Kasha's rule.[31−33] Our results uncover that the steric hindrance formed by a hydrogen bond (HB) exists in the NIR TADF emitter with the −CN group based on the independent gradient model (IGM) and the atom in the molecule (AIM) approaches,[34,35] resulting in a more twisted linkage plane of the ground state and the almost unchanged structure between excited states, thereby further permitting an extremely small driving force and internal reorganization energy, leading to a faster electron transfer rate in RISC and slower one in ISC. This work helps us understand the TADF mechanisms of CAT-1 molecule, which is beneficial for developing new efficient NIR TADF emitters.

2. METHODS

Recently, two molecules of 3-triphenylamine-4-cyano-acenaphtho[1,2-b]pyrazine-8,9-dicarbonitril (CAT-1) and 3-triphenylaminoacenaphtho[1,2-b]pyrazine-8,9-dicarbonitril, (TPAAP)[28,36] (Figure 1) have been synthesized and characterized by photophysical and photochemical methods. As clearly seen in Figure 1, the only difference between the two emitters comes from the additional functional group of cyano (−CN) in CAT-1. However, the fluorescence emission spectrum is dramatically different while it is quenched in the

deep red and NIR areas. As shown in Table 1 and refs 28 and 36, the emission wavelength for CAT-1 and TPAAP are 887 nm, and 705 nm, respectively. The two molecules have similar orders of k_{ISC}; however, for the RISC process, the rate of CAT-1 is 2 orders larger than TPAAP, although CAT-1 shows one-fifth of ΔE_{ST} than TPAAP. The photoluminescence quantum yield (PLQY) and the delayed fluorescence lifetime of CAT-1 and TPAAP in a toluene solution are 3.9%, 80 us and 97.3%, 6.9 ns, respectively.

It is well known that, in the Marcus equation, there are three parameters, namely, the Gibbs energy difference ΔG, which refers to the small exchange energy ΔE_{ST}; the reorganization energy λ, which can be generally decomposed into internal (vibrational reorganization energy λ_{in}) and external (solvent λ_{out}) contributions, while former arises from the changes in the geometry of the D and A units and the latter from changes in the electronic and nuclear polarization of the surrounding medium upon charge transfer; and the electronic coupling V between singlet and triplet excited states, described as the relativistic effect of the spin−orbit coupling (SOC). All these three parameters are used to determine the probability of the electron transfer process,[31,32] as shown in eq 1

$$k = \frac{|V|^2}{\hbar} \sqrt{\frac{\pi}{\lambda k_B T}} \exp\left[-\frac{(\Delta G + \lambda)^2}{4\lambda k_B T}\right] \tag{1}$$

where T is the temperature and k_B is the Boltzmann constant.

Starting from the ground states of these two TADF emitters, the ISC process can be regarded as the adiabatic reaction from the initial state S_1 to the final state T_1. In contrast, the RISC process is opposite to ISC with the adiabatic reaction occurring from the initial state T_1 to the final state S_1, as shown in Figure S1. In this case, the ISC rate k_{ISC} and RISC rate k_{RISC} are given by the Marcus formula. The expectation value of SOC for both ISC and RISC can be calculated by eqs 2 and 3

$$V_{ISC}^{IF} = \langle {}^1\psi_I^0 | H_{SO} | {}^3\psi_F^0 \rangle \tag{2}$$

$$V_{RISC}^{IF} = \langle {}^3\psi_F^0 | H_{SO} | {}^1\psi_I^0 \rangle \tag{3}$$

Herein, the geometric and electronic structures associated with singlet and triplet states were calculated by the DFT and TDDFT approaches. The structure−activity relationships (SARs) inferred from these studies help uncover the factors keeping emitters in longer emission wavelengths, which opens new ways for the rational design of TADF materials. To deeply understand the structures and electronic properties of CAT-1 and TPAAP, we specifically use a double-ζ def2-SVP basis set with the hybrid functionals M062X (56%), PBE0 (25% HF), and B3LYP (20%HF) to optimize the geometries since the excited state characteristics are sensitive to different Hartree−Fock (HF) exchange percentages.[37] In addition, the TDDFT approach is then adopted to construct nonadiabatic state excitation. The solvent effects have been carefully considered to obtain the best theoretical estimates, which can directly be compared with the experimental absorption and emission spectra. This effect is further mimicked using the solvation model based on density (SMD)[38] with toluene ($\varepsilon = 2.3741$). All of the calculations are implemented by Gaussian 09 program.[39]

3. RESULTS AND DISCUSSION

In the electronic structure calculations of the two TADF molecules, different functionals can heavily affect the accuracy of geometric prediction.[40] For the ground state geometry calculation, compared to HOMO/LUMO/E_g (eV) energy calculated by PBE0 and M062X functionals coupled with def2-SVP, it is found that B3LYP/def2-SVP predicts the best accordance with the experimental results, as shown in Table 1. For example, the calculated E_g is 1.68 eV for CAT-1 and 2.29 eV for TPAAP, which are quite well in agreement with the experimental measurements of 1.53 and 1.99 eV shown in Figure 2a and b, respectively. Therefore, the absorption and

Figure 2. Electrooptic properties of CAT-1 and TPAAP molecules. (a) Experimental (exp) and theoretical (theo) energies of S_1 (E_{S1}), T_1 (E_{T1}), and ΔE_{ST} of CAT-1 and TPAAP molecules. (b) Theoretical (black) and experimental (red) energy levels of the HOMO and LUMO, and frontier molecular orbital distributions.

emission wavelengths λ_{abs} and λ_{em}, respectively, calculated by B3LYP/def2-SVP are consistent with the experimental data listed in brackets. Furthermore, considering the excited-state energies are heavily dependent on the functionals in the TDDFT,[28,41] we have also adopted B3LYP, PBE0, and M062X to optimize the excited states. Table 1 reveals that the results of $E_S/E_T/\Delta E_{ST}$ calculated by B3LYP and PBE0 are consistent with the experimental data listed in brackets. Combined with the functional screening for the ground state structure,

B3LYP/def2-SVP was employed to predict all of the optoelectronic parameters of the two TADF molecules subsequently. The detailed photoabsorptions are illustrated in Figures S2−S5.

3.1. Gibbs Energy Difference and Reorganization Energy.

To unravel the ISC and RISC processes, we first focus on the Gibbs energy difference and reorganization energy. Since the ISC and RISC processes are carried out on the potential energy surface of the excited state, the corresponding structures of S_1 and T_1 are optimized first using TDDFT. As Figure 2b shows, HOMO is dominated by the donor unit and LUMO is determined by the acceptor unit.[42] As for the frontier orbital energy levels, good accordance with the experimental changing trend is evidenced. Similar phenomena are observed between the theoretical and experimental singlet and triplet energies. The ΔE_{ST} value of CAT-1 is smaller than that of TPAAP, indicating that the −CN group in CAT-1 can promote the reduction of driving force by regulating the adiabatic energy of excited states. Especially, compared with the value of 0.201 eV for TPAAP, ΔG for TADF emitter CAT-1 decreases rapidly to 0.002 eV, exhibiting an extremely small gap between S_1 and T_1, which ensures extremely small exchange energy (ΔE_{ST}) for the TADF design. Thus, the −CN group of CAT-1 can stabilize the adiabatic S_1 and T_1 at an energy level lower than that of TPAAP. Such a change in the excited state structure of CAT-1 is critical to the reorganization energy based on the Marcus theory and can be further calculated by the four-point model mentioned previously[43] (shown in Figure S1).

The λ_{in} and λ_{out} are considered to accurately describe the effect of reorganization energy. Since the computation of λ_{out} is quite difficult and varies significantly from the experimental results, the empirical values of 0.1 and 0.2 eV are used here for λ_{out}.[44] The λ_{in} is at least 2 orders of magnitude smaller than λ_{out} for CAT-1, indicating the dominating role of λ_{out} in affecting the transition rates between singlet and triplet states. For TPAAP, the λ_{in} is much larger than that of CAT-1, which could be attributed to the great linkage twists (Φ (C_1−C_2−C_3−C_4) displayed in Figure S6) change between the structure of S_1 and T_1 for TPAAP during the electron transition. As shown in Table S1, the twisting angle difference of S_1 and T_1 geometry in TPAAP is 23.7° (57.0° for S_1 and 33.3° for T_1), much larger than the twist difference of 0.4° in CAT-1 (89.1° for S_1 and 88.7° for T_1). To be more detailed, for CAT-1, the dihedral angle Φ from the S_0 state to the S_1 state changed by 32.6° (from 56.5° for S_0 to 89.1° for S_1), indicating the linkage twist with the perpendicular character after reaching the excited state. Meanwhile, the almost unchanged dihedral angle Φ of CAT-1 in the two excited states manifests that their excited geometries did not change much. For TPAAP, although the dihedral angle of the linkage twist between S_1 and T_1 states varies greatly, the linkage twist change is only 12.4° (from 44.6° for S_0 to 57.0° for S_1) from the S_0 state to the S_1 state, much smaller than that of CAT-1 with the change of 32.6°, manifesting less change in the geometry of TPAAP from the ground state to the excited state. Therefore, the extremely smaller λ_{in} of CAT-1 than that for TPAAP can be assigned to the little structural change between different excited states, which, as we infer, is related to the hydrogen bond (HB) formed by the cyano group (−CN).

3.1.1. Hydrogen Bond Steric Hindrance Analysis. Considering that the CN···H formation may limit the geometric

Table 2. Topological Parameters (in au) at BCPs of CAT-1[a]

states	bond length/Å	$\rho(r)$	$\Delta^2\rho_{(r)}$	$H(r)$	$V(r)$	$G(r)$	$H(r)/\rho(r)$
S_0	3.15	0.003	0.009	0.0005	−0.001	0.002	0.211
S_1/T_1	2.45	0.011	0.030	0.0006	−0.006	0.007	0.058

[a]$\rho(r)$, $\Delta^2\rho(r)$, $H(r)$, $V(r)$, $G(r)$, and $H(r)/\rho(r)$ are the electron density, Laplacian density, electronic energy density, potential energy density, Lagrangian kinetic density, and the ratio of $H(r)/\rho(r)$, respectively. All of the above quantities of units are au.
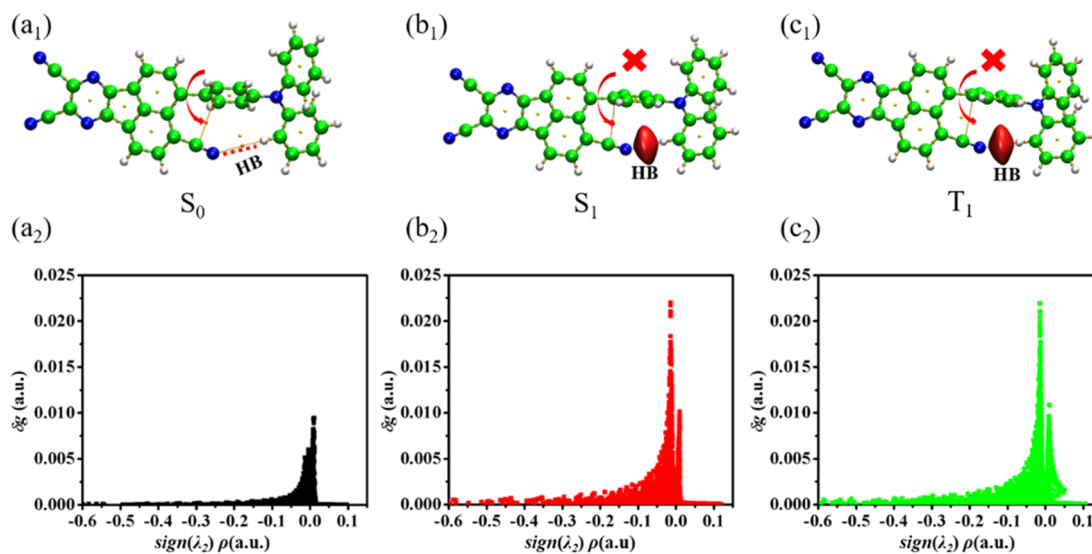
Figure 3. Hydrogen bond of molecule CAT-1 bearing the cyano group under the ground and excited states. (a_1), (b_1), and (c_1) IGM map and AIM graph of the intermolecular hydrogen bonding; the critical points of CAT-1 are represented by yellow circles and bond paths by an orange line. (a_1) $\delta g^{inter}(\rho) = 0.0025$ isosurface. (b_1) and (c_1) $\delta g^{inter}(\rho) = 0.0106$ isosurface. The red arrows in (a_1), (b_1), and (c_1) represent the possibility of the benzene linkage twist. (a_2), (b_2), and (c_2) are δg^{inter} two-dimensional (2-D) plots for the IGM models of structure S_0, S_1, and T_1, respectively.

change in the excited states, further affecting different photochemistry processes,[45] we further investigate the property of CN···H using the IGM and AIM theories. Both theories are introduced in the part of the Supporting Information. Table 2 lists the topological properties of the electron density at bond critical points (BCPs) ([3, −1] type). Interestingly, the distance between the −CN group and the associated hydrogen atom changed from 3.15 Å (for S_0 state) to 2.45 Å (for S_1/T_1 state). The positive $\Delta^2\rho(r)$ indicates no covalent bond between the cyano and corresponding hydrogen atoms. Based on the fact that the greater the $\rho(r)$ values with a more negative $V(r)$ at BCP, the stronger the bond,[46] and compared with these two values ($\rho(r)$ of 0.003 au., $V(r)$ of −0.001 au.) of the ground state S_0, the higher $\rho(r)$ (0.011 au) and negative $V(r)$ (−0.006 au) of the excited states S_1 and T_1 with a shorter CN···H distance can prove the HB formation in the structure of excited states. This speculation is evidenced again by the positive $H(r)$ and the radio $H(r)/\rho(r)$ that can explain the existence of a weak HB.

Such a weak HB can be represented by the topological properties, as displayed in Figure 3a_1, b_1, c_1. The red region is the $\rho(r)$ of the CN···H for CAT-1, which is very small in the ground state structure with a shallow δg^{inter} peak due to the long distance of the CN···H bond. However, the red region in the structure of the excited states is larger and has a higher δg^{inter} peak, demonstrating the strengthened HB tendency of the excited states. In Figure 3a_2, b_2, c_2, the $\rho(r)$, BCPs, and bonding paths of AIM are simultaneously drawn in a δg^{inter} isosurface map. Therefore, the whole process can be inferred as follows. When triggered by light pulses, the electrons in the ground state of CAT-1 are transferred to the excited state with

the structural change toward the formation of CN···H, leading to the benzene linkage gradually turning perpendicular to the plane of D and A units. Meanwhile, when the electrons are transferred between excited states (the ISC and RISC process), the HB can serve as a steric hindrance so that the corresponding linkage remains almost unchanged. Thus, for CAT-1, the reorganization energy between S_1 and T_1 is very small.

3.2. Electronic Coupling. The SOC is the key factor to control ISC and RISC. In the present work, the electronic coupling V between singlet and triplet excited states is calculated by B3LYP/def2-SVP with ORCA program[47] using the approximate one-electron spin−orbit Hamiltonian.[48,49] In addition to calculating the SOC value, the reliability of several approximate methods is also compared to evaluate the influence of hydrogen bond steric hindrance in the intersystem crossing process. Here, we mainly adopt the natural transition orbital (NTO) analysis and electronic density difference (EDD) method to further analyze the excited states controlled by the related ΔE_{ST} to the frontier orbital overlap, as well as the exciton characteristics properties with the same transition configurations.[50]

3.2.1. NTO Similarity Analysis. As a part of understanding the excited states of these emitters, the NTO analysis is employed to describe the exciton transformation based on the singular value decomposition of the one-particle transition density matrix.[51] Particularly, the highest occupied natural transition orbital (HONTO) and the lowest unoccupied natural transition orbital (LUNTO) excitation amplitudes are always the most significant for any particular excited state, owing to their dominating role in determining the one-electron
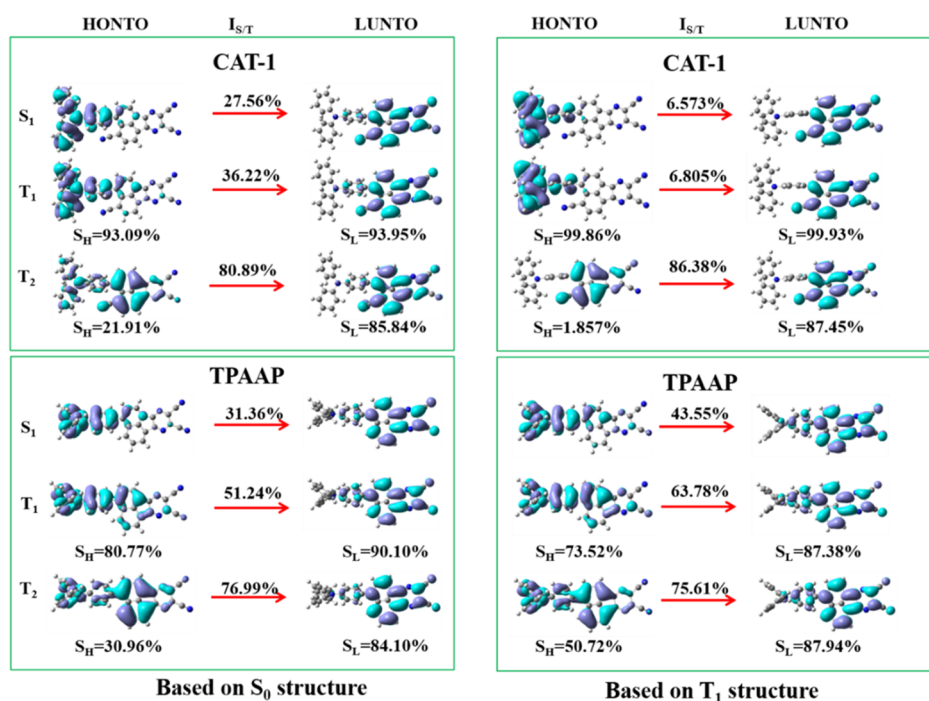
Figure 4. NTO analysis based on S_0 and T_1 structures for CAT-1. $I_{S/T}$ is the overlap degree of the single/triplet excited state. The left (right) scheme is an NTO analysis based on the S_0 (T_1) structure of the two TADF molecules.

transition from S_0 to the corresponding excited states. To further explore how the hydrogen bond steric hindrance affects the charge delocalization, TDDFT/B3LYP/def2-SVP is used to calculate the NTO for CAT-1 and TPAAP based on their optimized structure of the S_0 and T_1 states, as shown in Figure 4. The orbital similarity between HONTOs (s_H) and LUNTOs (s_L) is also calculated using Multiwfn.[52,53] The overlap degree I_S and I_T with a lower value represent the orbital with a higher portion of characteristic electron transfer state.

From the NTO analysis based on either the S_0 or T_1 structure for both S_1 and T_1 states, the large values of s_H and s_L indicate a high similarity of HONTOs and LUNTOs between the singlet and triplet excited states. The overlap degrees I_S and I_T of S_1 and T_1 in CAT-1 are lower than that in TPAAP based both on S_0 and T_1 structures, which means that the S_1 and T_1 in CAT-1 have less electron transfer character than those in TPAAP. While I_T of T_2 in CAT-1 is higher than that in TPAAP based on S_0 and T_1 structures, indicating that CAT-1 has more local excitation character for T_2 than that in TPAAP. Thus, the existence of hydrogen bond steric hindrance can inhibit the electron delocalization of CAT-1 in S_1 and T_1.

We further explore the influence of orbital change affected by hydrogen bond steric hindrance on the ISC rate. Based on Xu's research,[54] the values of $|s_H - s_L|$ represents the extent of orbital change during the exciton transformation. It has been confirmed that k_{ISC} could become faster when an orbital type changes during the ISC process.[54] Therefore, the difference between S_H and S_L values of HONTOs/LUNTOs for the excited states can be used to quantify the rate of the ISC process. As shown in Table 3, ($|s_H - s_L|$) based on the T_1 structure is 0.07% for CAT-1, which is much smaller than 13.86% of TPAAP. Such a trend is consistent with the experimental data that k_{ISC} of CAT-1 is smaller than that of TPAAP. Thus, the hydrogen bond steric hindrance can decrease the $|s_H - s_L|$, leading to a small k_{ISC} of CAT-1.

Table 3. Comparison of the NTO Analysis and SOC Values of the Investigated Molecules[a]

molecules		CAT-1	TPAAP
based on T_1	$|s_H - s_L|_{(S_1-T_1)}$	0.07%	13.86%
	$|s_H - s_L|_{(S_1-T_2)}$	85.59%	37.22%
	SOC $_{(S1-T1)}$ (cm^{-1})	0.020	0.058
	SOC $_{(S2-T1)}$ (cm^{-1})	0.054	0.005
	$k_{ISC}(\times 10^5)$	1.39	8.17

[a]Three types of parameters are used for the comparison: $|s_H - s_L|$, $|s_H + s_L|$, SOC, and k_{ISC}.

Moreover, the SOC between S_1 and T_1 for CAT-1 and TPAAP are 0.020 and 0.0576 cm^{-1}, respectively, manifesting the larger SOC representing the larger $|s_H - s_L|$ without the existence of hydrogen bond steric hindrance. Simultaneously, the SOC value of CAT-1 (0.054 cm^{-1}) between S_2 and T_1 is larger than that of TPAAP (0.005 cm^{-1}), indicating that orbital change in a higher excitation is not limited by the hydrogen bond steric hindrance, which also coincides well with the tendency of a larger $|s_H - s_L|$ value for CAT-1 than that for TPAAP. As shown in Table 3, the $|s_H - s_L|_{(S1-T2)}$ of CAT-1 and TPAAP are 85.59 and 37.22%, respectively, which have the same trend as the SOC $_{(S2-T1)}$ of the two molecules, and the SOC value of CAT-1 is almost 100 times larger than TPAAP.

3.2.2. Transition Configuration Analysis. Electronic density difference (EDD) analysis is another method of figuring out efficient ISC channels for exciton transformation,[55] and thus is used to further evaluate the influence of hydrogen bond steric hindrance. The TDDFT calculations can facilely obtain the EDD based on the S_0 structure. Besides, similar transition configurations and EDD of S_1 and T_1 are beneficial for the ISC. Therefore, within the allowable energy difference of $\pm$ 0.37 eV by the energy gap law, only one possible transition transfer from S_1 to T_n (T_1) for CAT-1 and two possible transition
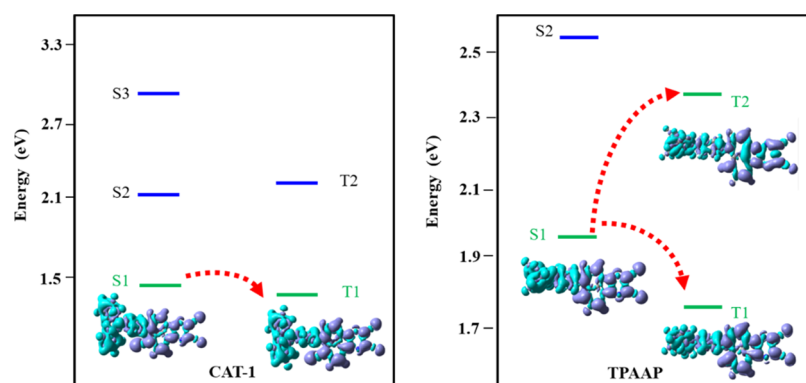
Figure 5. EDD of CAT-1 and TPAAP. The schema include the energy diagram, transition configuration, and electronic density transition analyses of the two molecules.

Table 4. ISC and RISC Rate Constants and SOC Matrix Elements of CAT-1 and TPAAP Molecules at B3LYP/def2-SVP Level[a]

	ISC				RISC		
molecules	ΔG (eV)	λ_{in} (meV)	k^b_{ISC} (10^5 s^{-1})	SOC (cm^{-1})	ΔG (eV)	λ_{in} (meV)	k^c_{RISC} (10^5 s^{-1})
CAT-1	−0.002	0.019	1.229, 0.331 (1.39[d])	0.020	0.002	0.067	1.139, 0.306 (0.14[d])
TPAAP	−0.201	127.4	17.31, 9.297 (8.17[d])	0.058	0.201	166.4	0.006, 0.003 0.002[d]

[a]The Gibbs energy difference ΔG, reorganization energy λ, electronic coupling V, and charge transfer rate k are listed in the table. [b]Calculated rate constant of intersystem crossing when λ_{out} = 0.1 eV and λ_{out} = 0.2 eV, respectively. [c]Calculated rate constants of reverse intersystem crossing when λ_{out} = 0.1 eV and λ_{out} = 0.2 eV, respectively. [d]The experimental data of ISC and RISC rate constants, respectively.

transfers for TPAAP, as shown in Figure 5. This includes the summarization of NTO and EDD analysis transition prediction. The electronic density of S_1 is very similar to T_1 for CAT-1, similar to that for TPAAP, with additional T_2 like S_1, which is agreeable with the exclusion of possible transition between the EDD beyond about ± 0.37 eV. Therefore, hydrogen bond steric hindrance has almost no effect on the EDD. Changes in NTO based on the S_0 and T_1 structures show the same changing trend as EDD: both molecules tend to transfer from S_1 to T_1. Even though the EDD reveals precisely no difference between CAT-1 and TPAAP, the NTO proves a more accessible approach for the intersystem crossing from S_1 to T_1 in TPAAP than in CAT-1.

3.3. ISC and RISC Rates. From the obtained λ, ΔG, and V, the ISC and RISC rates can be easily estimated from the Marcus formula eq 1. As displayed in Table 4, the molecule CAT-1 has a faster RISC rate and a slower ISC rate than TPAAP, which coincides well with the experimental data. The extremely small ΔG and the smaller λ_{in} caused by the hydrogen bond steric hindrance in CAT-1 are beneficial for prompting electron transition in excited states. Such steric hindrance is initiated by CN···H and can minimize the adiabatic energy of the single excited state and triplet excited state by reducing the corresponding structural changes when electron transfer occurs. In terms of λ_{out}, the calculated k_{ISC} and k_{RISC} agree with the experimental values when λ_{out} equals 0.1 and 0.2 eV. Furthermore, the smaller electronic coupling V of CAT-1 than that of TPAAP indicates that the singlet and triplet orbital spins can be regulated by introducing the steric hindrance in the TADF design to achieve the expected RISC rate. Hence, even though the photoluminescence behavior can be regulated by different phases,[56] it can also be regulated by hydrogen bond steric hindrance.

4. CONCLUSIONS

We have revealed the important influence of hydrogen bond steric hindrance on the ISC and RISC processes for the NIR TADF emitter with the photoluminescence (PL) close to 1000 nm. The calculated accuracy of Gibbs energy difference, electronic coupling, and internal and external reorganization energies entering the Marcus rate expression is discussed by comparing with the experimental results. The NTO and EDD analysis are introduced to further simulate the ISC rates quantitatively, demonstrating a more accessible approach for ISC from S_1 to T_1 in TPAAP than in CAT-1. We have found that the cyano group's hydrogen bond plays an essential role in the steric hindrance of the SAR that the geometry before and after the electron transfer has almost unchanged, leading to an extremely small internal reorganization energy and driving force. Meanwhile, such steric hindrance can cause the plane to be twisted and further inhibit electron delocalization. Compared with the smaller electron coupling, the extremely smaller reorganization energy and driving force generated by the hydrogen bond steric hindrance can lead to a faster electron transfer rate in RISC and a slower rate in ISC. Even though the molecules in the NIR region have a relatively low ISC rate, the faster RISC rate with near-infrared PL characteristics is extremely desirable for designing novel NIR TADF emitters. Hence, the hydrogen bond steric hindrance is a conceptually useful guide to the experimental synthesis of novel NIR TADF design.

■ ASSOCIATED CONTENT

ⓈI Supporting Information

The Supporting Information is available free of charge at https://pubs.acs.org/doi/10.1021/acs.jpca.1c00739.

> Mechanism of electron transfer process on potential energy surface (Part 1); the comparison of the calculated spectrum and the experimental spectrum (Part 2); analysis of electronic excited states distribution (Part 3);

F

and the dihedral angle Φ of $C_1-C_2-C_3-C_4$ and its comparison between the ground state and the excited states of two TADF molecules (Part 4) (PDF)

■ AUTHOR INFORMATION

Corresponding Authors

Yubing Si − College of Chemistry, Zhengzhou University, Zhengzhou 450001, China; ● orcid.org/0000-0003-3593-5941; Email: ybsi@zzu.edu.cn

Keqin Li − College of Computer Science and Electronic Engineering, Hunan University, Changsha 410082, China; Department of Computer Science, State University of New York, New Paltz, New York 12561, United States; Email: lik@newpaltz.edu

Authors

Can Leng − Science and Technology on Parallel and Distributed Processing Laboratory and Laboratory of Software Engineering for Complex Systems, National University of Defense Technology, Changsha 410073, China; National Supercomputer Center in Changsha, Changsha 410082, China; ● orcid.org/0000-0003-0632-7429

Sheng You − National Supercomputer Center in Changsha, Changsha 410082, China

Hai-Mei Qin − College of Chemistry and Chemical Engineering, Fujian Provincial Key Laboratory of Theoretical and Computational Chemistry, Xiamen University, Xiamen 361005, China

Jie Liu − Science and Technology on Parallel and Distributed Processing Laboratory and Laboratory of Software Engineering for Complex Systems, National University of Defense Technology, Changsha 410073, China

Wei-Qing Huang − Department of Applied Physics, School of Physics and Electronics, Hunan University, Changsha 410082, China; ● orcid.org/0000-0002-9621-8332

Complete contact information is available at:
https://pubs.acs.org/10.1021/acs.jpca.1c00739

Notes

The authors declare no competing financial interest.

■ REFERENCES

(1) Congreve, D. N.; Lee, J.; Thompson, N. J.; Hontz, E.; Yost, S. R.; Reusswig, P. D.; Bahlke, M. E.; Reineke, S.; Van Voorhis, T.; Baldo, M. A. External Quantum Efficiency above 100% in a Singlet-Exciton-Fission-Based Organic Photovoltaic Cell. *Science* **2013**, *340*, 334−337.

(2) Xuan, J.; Xiao, P. D. W.-J. Visible-Light Photoredox Catalysis. *Angew. Chem., Int. Ed.* **2012**, *51*, 6828−6838.

(3) Prasadhari, D.; Burkhard, K. Synthetic Applications of Eosin Y in Photoredox Catalysis. *Chem. Commun.* **2014**, *45*, 6688−6699.

(4) Yang, Z.; Mao, Z.; Xie, Z.; Zhang, Y.; Liu, S.; Zhao, J.; Xu, J.; Chi, Z.; Aldred, M. P. Recent Advances in Organic Thermally Activated Delayed Fluorescence Materials. *Chem. Soc. Rev.* **2017**, *46*, 915−1016.

(5) Uoyama, H.; Goushi, K.; Shizu, K.; Nomura, H.; Adachi, C. Highly Efficient Organic Light-Emitting Diodes from Delayed Fluorescence. *Nature* **2012**, *492*, 234−238.

(6) Adachi, C. Third-Generation Organic Electroluminescence Materials. *Jpn. J. Appl. Phys.* **2014**, *53*, 060101−060111.

(7) Tao, Y.; Yuan, K.; Chen, T.; Xu, P.; Li, H.; Chen, R.; Zheng, C.; Zhang, L.; Huang, W. Thermally Activated Delayed Fluorescence Materials Towards the Breakthrough of Organoelectronics. *Adv. Mater.* **2014**, *26*, 7931−7958.

(8) Li, Y.; Li, X.-L.; Chen, D.; Cai, X.; Xie, G.; He, Z.; Wu, Y.-C.; Lien, A.; Cao, Y.; Su, S.-J. Design Strategy of Blue and Yellow Thermally Activated Delayed Fluorescence Emitters and Their All-Fluorescence White Oleds with External Quantum Efficiency Beyond 20%. *Adv. Funct. Mater.* **2016**, *26*, 6904−6912.

(9) Zheng, Z.; Manna, A. K.; Hendrickson, H. P.; Hammer, M.; Song, C.; Geva, E.; Dunietz, B. D. Molecular structure, spectroscopy, and photoinduced kinetics in trinuclear cyanide bridged complex in solution: a first-principles perspective. *J. Am. Chem. Soc.* **2014**, *136*, 16954−16957.

(10) Minaev, B.; Baryshnikov, G.; Agren, H. Principles of Phosphorescent Organic Light Emitting Devices. *Phys. Chem. Chem. Phys.* **2014**, *16*, 1719−1758.

(11) Front Matter. In *Highly Efficient Oleds with Phosphorescent Materials*; Yersin, H., Ed.; Academic: Wiley-Vch: 2007.

(12) Tanaka, H.; Shizu, K.; Miyazaki, H.; Adachi, C. Efficient Green Thermally Activated Delayed Fluorescence (Tadf) from a Phenoxazine−Triphenyltriazine (Pxz−Trz) Derivative. *Chem. Commun.* **2012**, *48*, 11392−11394.

(13) Zhang, D.; Duan, L.; Li, C.; Li, Y.; Li, H.; Zhang, D.; Qiu, Y. High-Efficiency Fluorescent Organic Light-Emitting Devices Using Sensitizing Hosts with a Small Singlet−Triplet Exchange Energy. *Adv. Mater.* **2014**, *26*, 5050−5055.

(14) Lei, Z.; Sun, C.; Pei, P.; Wang, S.; Li, D.; Zhang, X.; Zhang, F. Stable, Wavelength-Tunable Fluorescent Dyes in the Nir-Ii Region for in Vivo High-Contrast Bioimaging and Multiplexed Biosensing. *Angew. Chem. Int. Ed.* **2019**, *58*, 8166−8171.

(15) Kim, J. H.; Yun, J. H.; Lee, J. Y. Recent Progress of Highly Efficient Red and near-Infrared Thermally Activated Delayed Fluorescent Emitters. *Adv. Opt. Mater.* **2018**, *6*, No. 1800255.

(16) Zampetti, A.; Minotto, A.; Cacialli, F. Near-Infrared (Nir) Organic Light-Emitting Diodes (Oleds): Challenges and Opportunities. *Adv. Funct. Mater.* **2019**, *29*, No. 1807623.

(17) Yang, T.; Liang, B.; Cheng, Z.; Li, C.; Lu, G.; Wang, Y. Construction of Efficient Deep-Red/near-Infrared Emitter Based on a Large Π-Conjugated Acceptor and Delayed Fluorescence Oleds with External Quantum Efficiency of over 20%. *J. Phys. Chem. C* **2019**, *123*, 18585−18592.

(18) Liang, Q.; Xu, J.; Xue, J.; Qiao, J. Near-Infrared-Ii Thermally Activated Delayed Fluorescence Organic Light-Emitting Diodes. *Chem. Commun.* **2020**, *56*, 8988−8991.

(19) Hu, T.; Tu, Z.; Han, G.; Yi, Y. Origin of High-Efficiency near-Infrared Organic Thermally Activated Delayed Fluorescence: The Role of Electronic Polarization. *J. Phys. Chem. C* **2021**, *125*, 1249−1255.

(20) Lee, S. Y.; Yasuda, T.; Nomura, H.; Adachi, C. High-Efficiency Organic Light-Emitting Diodes Utilizing Thermally Activated Delayed Fluorescence from Triazine-Based Donor−Acceptor Hybrid Molecules. *Appl. Phys. Lett.* **2012**, *101*, No. 093306.

(21) Jankus, V.; Data, P.; Graves, D.; McGuinness, C.; Santos, J.; Bryce, M. R.; Dias, F. B.; Monkman, A. P. Highly Efficient Tadf Oleds: How the Emitter−Host Interaction Controls Both the Excited State Species and Electrical Properties of the Devices to Achieve near 100% Triplet Harvesting and High Efficiency. *Adv. Funct. Mater.* **2014**, *24*, 6178−6186.

(22) Shizu, K.; Tanaka, H.; Uejima, M.; Sato, T.; Tanaka, K.; Kaji, H.; Adachi, C. Strategy for Designing Electron Donors for Thermally Activated Delayed Fluorescence Emitters. *J. Phys. Chem. C* **2015**, *119*, 1291−1297.

(23) Wang, K.; Liu, W.; Zheng, C. J.; Shi, Y. Z.; Liang, K.; Zhang, M.; Ou, X. M.; Zhang, X. H. A Comparative Study of Carbazole-Based Thermally Activated Delayed Fluorescence Emitters with Different Steric Hindrance. *J. Mater. Chem. C* **2017**, 4797−4803.

(24) Kim, D.-H.; et al. High-Efficiency Electroluminescence and Amplified Spontaneous Emission from a Thermally Activated Delayed Fluorescent near-Infrared Emitter. *Nat. Photonics* **2018**, *12*, 98−104.

(25) Ye, H.; et al. Near-Infrared Electroluminescence and Low Threshold Amplified Spontaneous Emission above 800 Nm from a Thermally Activated Delayed Fluorescent Emitter. *Chem. Mater.* **2018**, *30*, 6702−6710.

(26) Yuan, Y.; Hu, Y.; Zhang, Y.-X.; Lin, J.-D.; Wang, Y.-K.; Jiang, Z.-Q.; Liao, L.-S.; Lee, S.-T. Over 10% EQE near-Infrared Electroluminescence Based on a Thermally Activated Delayed Fluorescence Emitter. *Adv. Funct. Mater.* **2017**, *27*, No. 1700986.

(27) Wang, C.; et al. Highly Efficient Nondoped Green Organic Light-Emitting Diodes with Combination of High Photoluminescence and High Exciton Utilization. *ACS Appl. Mater. Interfaces* **2016**, *8*, 3041−3049.

(28) Congrave, D. G.; Drummond, B. H.; Conaghan, P. J.; Francis, H.; Jones, S. T. E.; Grey, C. P.; Greenham, N. C.; Credgington, D.; Bronstein, H. A Simple Molecular Design Strategy for Delayed Fluorescence toward 1000 Nm. *J. Am. Chem. Soc.* **2019**, *141*, 18390−18394.

(29) Patterson, J. D. *Density-Functional Theory of Atoms and Molecules*; Parr, R. G.; Yang, W., Eds.; Oxford University Press: New York, and Clarendon Press: Oxford, 1989.

(30) Runge, E.; Gross, E. K. U. Density-Functional Theory for Time-Dependent Systems. *Phys. Rev. Lett.* **1984**, *52*, 997−1000.

(31) Marcus, R. A. On the Theory of Oxidation—Reduction Reactions Involving Electron Transfer. V. Comparison and Properties of Electrochemical and Chemical Rate Constants1. *J. Phys. Chem. A* **1963**, *67*, 853−857.

(32) Marcus, R. A.; Sutin, N. Electron Transfers in Chemistry and Biology. *Biochim. Biophys. Acta, Rev. Bioenerg.* **1985**, *811*, 265−322.

(33) Kasha, M. Characterization of Electronic Transitions in Complex Molecules. *Discuss. Faraday Soc.* **1950**, *9*, 14−19.

(34) Ransil, B. J. Studies in Molecular Structure. Iv. Potential Curve for the Interaction of Two Helium Atoms in Single-Configuration Lcao Mo Scf Approximation. *J. Chem. Phys.* **1961**, *34*, 2109−2118.

(35) Bader, R. F. W. *Atoms in Molecules: A Quantum Theory*; Journal of Molecular Structure: THEOCHEM; Clarendon Press, 1994; Vol. *360*, pp 1−3.

(36) Xue, J.; Liang, Q.; Wang, R.; Hou, J.; Li, W.; Peng, Q.; Shuai, Z.; Qiao, J. Highly Efficient Thermally Activated Delayed Fluorescence Via J-Aggregates with Strong Intermolecular Charge Transfer. *Adv. Mater.* **2019**, *31*, No. 1808242.

(37) Huang, S.; Zhang, Q.; Shiota, Y.; Nakagawa, T.; Kuwabara, K.; Yoshizawa, K.; Adachi, C. Computational Prediction for Singlet- and Triplet-Transition Energies of Charge-Transfer Compounds. *J. Chem. Theory Comput.* **2013**, *9*, 3872−3877.

(38) Marenich, A. V.; Cramer, C. J.; Truhlar, D. G. Universal Solvation Model Based on Solute Electron Density and on a Continuum Model of the Solvent Defined by the Bulk Dielectric Constant and Atomic Surface Tensions. *J. Phys. Chem. B* **2009**, *113*, 6378−6396.

(39) Frisch, M.; Trucks, G.; Schlegel, H.; Scuseria, G.; Robb, M.; Cheeseman, J.; Scalmani, G.; Barone, V.; Mennucci, B.; Petersson, G.. *Gaussian09*, Revision D.01; Gaussian. Inc.: Wallingford, CT, 2009.

(40) Zheng, Z.; Brédas, J.; Coropceanu, V. Description of the charge transfer states at the pentacene/c60 interface: combining range-separated hybrid functionals with the polarizable continuum model. *J. Phys. Chem. Lett.* **2016**, *7*, 2616−2621.

(41) Pandey, L.; Doiron, C.; Sears, J. S.; Brédas, J.-L. Lowest Excited States and Optical Absorption Spectra of Donor−Acceptor Copolymers for Organic Photovoltaics: A New Picture Emerging from Tuned Long-Range Corrected Density Functionals. *Phys. Chem. Chem. Phys.* **2012**, *14*, 14243−14248.

(42) Wu, T.-L.; Huang, M.-J.; Lin, C.-C.; Huang, P.-Y.; Chou, T.-Y.; Chen-Cheng, R.-W.; Lin, H.-W.; Liu, R.-S.; Cheng, C.-H. Diboron Compound-Based Organic Light-Emitting Diodes with High Efficiency and Reduced Efficiency Roll-Off. *Nat. Photonics* **2018**, *12*, 235−240.

(43) Nelsen, S. F.; Blackstock, S. C.; Kim, Y. Estimation of Inner Shell Marcus Terms for Amino Nitrogen Compounds by Molecular Orbital Calculations. *J. Am. Chem. Soc.* **1987**, *109*, 677−682.

(44) Schmidt, K.; et al. Intersystem Crossing Processes in Nonplanar Aromatic Heterocyclic Molecules. *J. Phys. Chem. A* **2007**, *111*, 10490−10499.

(45) Zhao, G.-j.; Han, K.-L. Hydrogen Bonding in the Electronic Excited State. *Acc. Chem. Res.* **2012**, *45*, 404−413.

(46) Espinosa, E.; Alkorta, I.; Elguero, J.; Molins, E. From Weak to Strong Interactions: A Comprehensive Analysis of the Topological and Energetic Properties of the Electron Density Distribution Involving X-H⋯F-Y Systems. *J. Chem. Phys.* **2002**, *117*, 5529−5542.

(47) Neese, F. Software Update: The Orca Program System, Version 4.0. *WIREs Comput. Mol. Sci.* **2018**, *8*, No. e1327.

(48) Marian, C. M. Spin-Orbit Coupling and Intersystem Crossing in Molecules. *Wiley Interdiscip. Rev.: Comput. Mol. Sci.* **2012**, *2*, 187−203.

(49) Cui, G.; Thiel, W. Generalized Trajectory Surface-Hopping Method for Internal Conversion and Intersystem Crossing. *J. Chem. Phys.* **2014**, *141*, No. 124101.

(50) Chen, T.; Zheng, L.; Yuan, J.; An, Z.; Chen, R.; Tao, Y.; Li, H.; Xie, X.; Huang, W. Understanding the Control of Singlet-Triplet Splitting for Organic Exciton Manipulating: A Combined Theoretical and Experimental Approach. *Sci. Rep.* **2015**, *5*, No. 10923.

(51) Kim, D.; Coropceanu, V.; Brédas, J.-L. Design of Efficient Ambipolar Host Materials for Organic Blue Electrophosphorescence: Theoretical Characterization of Hosts Based on Carbazole Deriva-tives. *J. Am. Chem. Soc.* **2011**, *133*, 17895−17900.

(52) Lu, T.; Chen, F. Multiwfn: A Multifunctional Wavefunction Analyzer. *J. Comput. Chem.* **2012**, *33*, 580−592.

(53) Lu, T.; Chen, F. Quantitative Analysis of Molecular Surface Based on Improved Marching Tetrahedra Algorithm. *J. Mol. Graphics Modell.* **2012**, *38*, 314−323.

(54) Xu, S.; Yang, Q.; Wan, Y.; Chen, R.; Wang, S.; Si, Y.; Yang, B.; Liu, D.; Zheng, C.; Huang, W. Predicting Intersystem Crossing Efficiencies of Organic Molecules for Efficient Thermally Activated Delayed Fluorescence. *J. Mater. Chem. C* **2019**, *7*, 9523−9530.

(55) An, Z.; et al. Stabilizing Triplet Excited States for Ultralong Organic Phosphorescence. *Nat. Mater.* **2015**, *14*, 685−690.

(56) Wang, C.; Liu, Y.; Feng, X.; Zhou, C.; Liu, Y.; Yu, X.; Zhao, G. Phase Regulation Strategy of Perovskite Nanocrystals from 1DOrthomorphic NH_4PbI_3 to 3D Cubic $(NH_4)_{0.5}Cs_{0.5}Pb(I_{0.5}Br_{0.5})_3$ Phase Enhances Photoluminescence. *Angew. Chem., Int. Ed.* **2019**, *58*, 11642−11646.